OPEN

NPG Asia Materials (2015) 7, e215; doi:10.1038/am.2015.98

www.nature.com/am

ORIGINAL ARTICLE

Mimicking how plants control CO_2 influx: CO_2 activation of ion current rectification in nanochannels

Yanglei Xu[1], Minghui Zhang[1], Tong Tian, Ying Shang, Zheyi Meng, Jiaqiao Jiang, Jin Zhai and Yao Wang

One of the key processes of photosynthesis is to control the influx of atmospheric carbon dioxide (CO_2). Ion channels fulfill this process by regulating the opening and closing of stomatal pores in plants' leaves. Inspired by this natural process, we have developed an amidine-modified gas-responsive system that closely mimics stomatal pores: CO_2 rather than the variation in the pH value directly modulates the conductance state of the channel. The CO_2-activated chemical reaction of amidine groups is reversible and produces an excess surface charge on the pore walls of asymmetric nanochannels, which makes the ions pass preferentially through the nanochannels in one direction relative to the conductance in the other direction, resulting in a significant ion current rectification. Furthermore, the influence of the different molecular conformation of the amidine-containing molecules on the current is investigated and discussed. The conclusive simulation of our system based on the Poisson and Nernst–Planck (PNP) model is also in good agreement with the experimental results. Accordingly, we have successfully mimicked the mechanism of stomatal closure in plants with our gas-activated nanosystem.
NPG Asia Materials (2015) **7,** e215; doi:10.1038/am.2015.98; published online 11 September 2015

INTRODUCTION

Carbon dioxide (CO_2) has become one of the most advanced and heavily studied topics internationally in fields related to energy and the environment.[1–3] In nature, there is an intimate relationship between CO_2 gas and fluidic ion channels.[4] Ion channels located within the plasma membrane of cells control the flow of ions across cell membranes.[5] An example of CO_2-activated biological ion channels is that of plasma-membrane anion channels in plants, whereby CO_2 directly modulates the activity of the anion channels in stomatal aperture during the photosynthesis process.[6,7] Rises in the partial pressure of CO_2 cause rapid increases in the activity of the transmembrane anion channel, which leads to the closure of stomatal pores in leaves to prohibit CO_2 influx into plants. The transmembrane anion channel mentioned above is denoted as *slow anion channel-associated 1* (*slac1*),[8] which facilitates anion efflux flow when the CO_2 level is high. In summary, *slac1* controls this response reversibly with a mechanism in which the CO_2 gas directly activates anion channel regulation. Inspired by this natural process, we constructed an artificial smart system that presents a similar regulation mechanism by directly reacting with CO_2.

Ion channels exhibit the unique behavior of ion current rectification;[9] that is, ions pass preferentially through nanochannels in one direction relative to the conductance in the other direction.[10–13] Because biological ion channels are difficult to reproduce in practice due to their fragile components and the strict lipid bi-layer environment required, constructing robust artificial nanochannels[14] to mimic this natural behavior provides a solution. In recent decades, ionic nanochannels have attracted considerable attention due to their broad range of applications,[15–17] such as biosensing and energy conversion. Nevertheless, most previous studies on rectification have been based on liquid–solid interactions.[18–23] The gas phase in the nanofluidic system was not recognized until it was reported in 2011 that the physical loading of gas pressure also influences the rectification property of the nanofluidic system,[24] although this work considered physically driven rectification, and it is hard to distinguish the components of the gas.

In this work, we demonstrate CO_2-induced ion gating in nanochannels, which is induced by a CO_2-activated chemical reaction and is consistent with stomatal closure in response to CO_2. As shown in Figure 1a, during the photosynthesis of plants, CO_2 causes the reversible activation of anion channels.[25] The reaction of CO_2, H_2O and transmembrane proteins forms protons and bicarbonate under the catalysis of carbonic anhydrase, which causes a conformational change in transmembrane proteins. Hence, CO_2 is sensed by the plants to adjust the opening of these pores and induce anion transport from one side of the membrane to the other.[26] Similarly, we developed artificial ion channels that utilize two amidine-containing[27–33] molecules with flexible and rigid molecular structures located on the inner wall of the channels to regulate the ion current. The reaction of CO_2 with amidine groups leads to the conversion of CO_2, water and

Key Laboratory of Bio-Inspired Smart Interfacial Science and Technology of Ministry of Education, Key Laboratory of Beijing Energy, School of Chemistry and Environment, Beihang University, Beijing, China
[1]These authors contributed equally to this work.
Correspondence: Professor J Zhai or Professor Y Wang, Key Laboratory of Bio-Inspired Smart Interfacial Science and Technology of Ministry of Education, Key Laboratory of Beijing Energy, School of Chemistry and Environment, Beihang University, No.37, Xueyuan Road, Haidian District, Beijing 100191, China.
E-mail: zhaijin@buaa.edu.cn or yao@buaa.edu.cn
Received 8 January 2015; revised 18 June 2015; accepted 28 June 2015

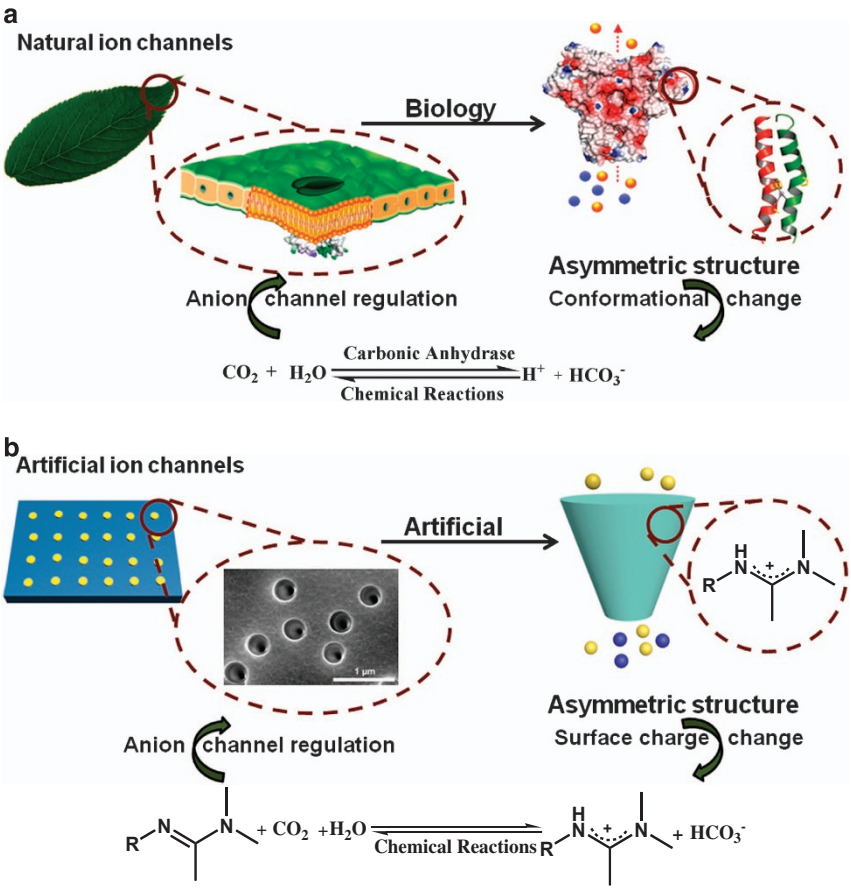

Figure 1 Scheme of the (**a**) biological and (**b**) bio-inspired CO_2-activated and chemical-driven anion-selective ion channels. These smart systems result in anion channel regulation based on the mechanism of the chemical reaction of CO_2. (**a**) In green plant cells, the reaction of CO_2 inside ion channels under the catalysis of carbonic anhydrase causes a conformational change in transmembrane proteins, and the anions pass through the ion channels preferentially from one side to the other due to the asymmetric shape of the protein. (**b**) In the artificial nanochannel system, the reaction of CO_2 inside ion channels under the reaction of amidine groups causes the surface charge to change from neutral to positive, and the anions preferentially pass through the nanochannels from the tip to the base due to the asymmetric conical shape.

amidine groups to bicarbonate and amidine cations. As illustrated in Figure 1b, the variation in amidine charge changes the surface charge of the nanochannels from neutral to positive. Thus, the anions can pass preferentially through the nanochannels. As a result, with the synergism between the conical asymmetric shape and the peculiar nanoenvironment of the positively charged surface, artificial nanochannel systems can show rectification properties. Because the chemical reaction of amidine groups with CO_2 is reversible, ventilation with N_2 initiates the reverse reaction and makes the rectification properties of the nanochannels vanish, as expected.

MATERIALS AND METHODS

Nanochannel fabrication

The conical-shaped nanochannels were produced in polyethylene terephthalate membrane (PET, Hostaphan RN12 Hoechst, GSI, Darmstadt, Germany, 23-μm thick) using a well-developed ion track-etching technique.[34] Before the chemical etching process, the sample of the PET membrane was exposed to ultraviolet light for 1 h on each side. The voltage (1 V) was used to monitor the etching process such that the transmembrane ionic current could be observed as soon as the nanochannel opened. Both sides of the cell were added to a solution that was able to neutralize the etchant as soon as the nanochannel opened, thus slowing down the etching process. The following are the etching and stopping solutions for the etching of PET: 9 M NaOH for etching, 1 M KCl and 1 M HCOOH for stopping. The large side of the conical nanochannel is called the base, and the small side is called the tip. The large opening (base) was ~300 nm in diameter, and the tip diameter was ~10 nm, as measured with electrochemical methods. Ion currents were measured using a Keithley 6487 picoammeter. For this work, the PET film was set-up between the two halves of the cell and filled with an electrolyte solution of 0.1 M KCl. Then, the measurements were carried out.

Synthesis of DEPBA

DEPBA (4-[4-(1-dimethylamino-ethylideneamino)-phenyl-butyric acid) was synthesized by Scoggins' route. 4-(4-Aminophenyl)butyric acid (0.6 g, 3.35 mmol) and dimethylacetamide dimethyl acetal (0.98 ml, 7 mmol) were stirred with 15 ml dimethylformamide at 65 °C for 1 h under an N_2 atmosphere. The removal of solvent under reduced pressure, followed by chromatography using a silica gel column ($CHCl_3$:MeOH:NH_3H_2O, 2.00:2.90:0.08, v:v, Rf = 0.35) afforded 0.56 g of DEPBA as an orange liquid (67%) with 1H-NMR (p.p.m., 400 MHz, DMSO-d6) δ7.02-6.96 (m, 2H), 6.52-6.46 (m, 2H), 2.94-2.90 (s, 6H), 2.54-2.48 (m, 2H), 2.16-2.10 (m, 2H), 1.80-1.78 (s, 3H), 1.78-1.70 (m, 2H).

Synthesis of DEDA

DEDA (12-(1-Dimethylamino-ethylideneamino)-dodecanoic acid) was synthesized by Scoggins' route. A solution of 12-aminolauric acid (0.2153 g, 1 mmol) and dimethylacetamide dimethyl acetal (0.32 ml) was stirred at 65 °C for 30 min in 9 ml of methanol under an N_2 atmosphere. After cooling down to room temperature, the solvent was evaporated under reduced pressure. Chloroform

was added, and the resulting solution was washed by water three times. Finally, the solvent was removed, and the end product was dried in a vacuum.

DEPBA and DEDA immobilization

(Supplementary Figure S14) Step 1: after chemical etching, the carboxyl groups were on the surface. Step 2: the PET film was first exposed to an aqueous solution of 1-ethyl-3-(3-dimethylaminopropyl) carbodiimide hydrochloride (EDC·HCl) 100 mM) and pentafluorophenol (PFP, 100 mM) for 1 h. Then, 0.1 ml ethylenediamine anhydrous (EDA) was added to the solution and reacted for 4 h at room temperature. Step 3: the film was reacted with an ethanol solution containing DEPBA or DEDA (20 mM), EDC·HCl (50 mM) for 1 day. The film was washed with thoroughly deoxygenated MilliQ water (Millipore, Boston, MA, USA) (18.2 MΩ) before current–voltage (*I–V*) measurement.

Current measurement

The ionic transport properties of the nanochannel were studied by measuring the ionic current through the nanochannels. The ionic current was measured using a Keithley 6487 picoammeter (Keithley Instruments, Cleveland, OH, USA). The main transmembrane potential used in this work was evaluated, and a scanning voltage that varied from −2 to 2 V and a 40-s period was selected. Current values were obtained from 5–10 independent measurements, and the error in each case was ±5%. The membrane was bubbled with CO_2 in water before current measurement. When conducting the reverse reaction, the membrane was ventilated with N_2 in air without water for 30 min. CO_2 flow rate: 20 ml s^{-1}. Error bars are given by the s.d. of five measurements under the same conditions.

XPS and infrared test

X-ray photoelectron spectroscopy analysis (XPS) and a Fourier transform infrared microscope were used to detect the levels of DEPBA or DEDA to confirm the successful modification on the PET surface. XPS data were obtained with an ESCA Lab 220i-XL electron spectrometer from VG Scientific using 300 W Al Kα radiations. The base pressure was $\sim 3 \times 10^{-9}$ mbar. The binding energies were referenced to the C1s line at 284.8 eV from adventitious carbon. The Fourier transform infrared spectra were measured on a Thermo Scientific infrared spectrometer in the 400–4000 cm^{-1} region.

RESULTS

Amidine-containing molecules of DEPBA and DEDA were synthesized by Scoggins' route[35,36] (Supplementary Figures S1 and S2). The interior surface of the nanochannels was modified with DEPBA or DEDA using a three-step coupling reaction.[37] EDA was covalently coupled to the surface to introduce -NH_2 functional groups after activation with EDC·HCl and PFP. Subsequently, the interior surface of the nanochannels was modified by DEPBA or DEDA. In the infrared spectrum of the membrane before and after DEPBA or DEDA modification, six characteristic peaks of PET (1710, 1250, 1162, 1135, 1090 and 816 cm^{-1}) were observed. The characteristic bands in region 3399 cm^{-1} can be regarded as features of the EDA group. The characteristic bands in the region from 1630 cm^{-1} can be regarded as features of the amidine group. (Supplementary Figure S3). XPS analysis was used to detect the content of nitrogen contained in DEPBA or DEDA. As shown in Supplementary Figures S4 and S5, the appearance of an N1s signal on the PET surface after modification confirms the successful attachment of DEPBA or DEDA on the PET surface. The ion transport properties of the nanochannels before and after modification were examined by current measurements. Figure 2 shows the corresponding *I–V* curves of each step of the modification process. Before modification, the pristine negatively charged carboxyl groups attract the cations to neutralize the immobilized surface charge at pH 4.0. The cations prefer to pass from the tip to the base to maintain lower resistance, resulting in current rectification

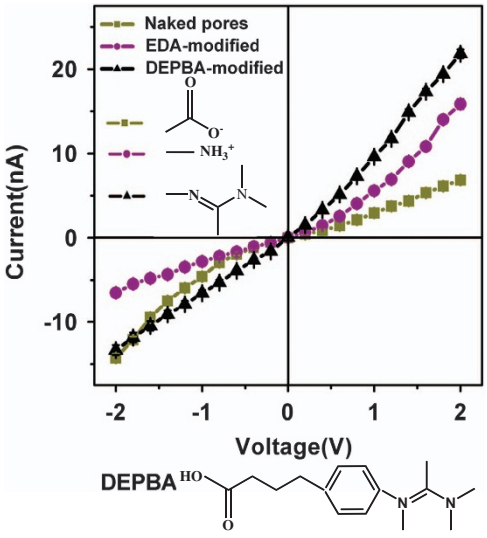

Figure 2 The corresponding current–voltage *(I–V)* curves of the modification process. The PET membrane was placed between two halves of electrolyte using a 0.1 M KCl electrolyte solution at pH 4.0. EDA, ethylenediamine anhydrous; DEPBA, 4-[4-(1-dimethylamino-ethylideneamino)-phenyl-butyric acid.

properties.[38] Ion channels have unique behaviour of ion current rectification, that is, ions pass preferentially through the nanochannels in one direction relative to the conductance in the other direction, which is reported as ion current rectification.[39] The rectification ratio (the ratio of absolute values of currents at a given voltage 2 V versus −2 V) is ~0.72. When carboxyl groups were converted to amino groups, the nanochannels varied from cation selective to anion selective at pH 4, and the direction of rectification was the opposite. The rectification ratio is ~2.44. After modification with DEPBA, the rectification ratio is ~1.64 due to little surface charge on the surface. Supplementary Figure S6 shows the ion current change of the DEDA-modification progress.

Figure 3a shows the corresponding *I–V* curves of the reaction process of CO_2 and N_2. After bubbling CO_2 in water, the ion current was reduced to ~11.96 nA at 2 V and to ~−2.60 nA at −2 V, and the rectification ratio greatly increased to ~4.60, indicating that the reaction of CO_2 with DEPBA caused the surface charge to change from neutral to positive. The reaction of CO_2 in ion channels is reversible. The ventilation of the system with N_2 in the absence of H_2O induces ion current to return to the original value, which is due to the reverse reaction of DEPBA with CO_2. Supplementary Figure S7 shows the change to *I–V* curves in DEDA-modified ion channels after bubbling CO_2 or N_2 to the nanochannels. Figure 3b shows the conductance reversibility of this smart nanochannel system on alternating the gas component of CO_2 and N_2. The reversibility and repeatability of the reaction process are demonstrated by monitoring the conductance at +2 V and −2 V, on sequential exposure of the DEPBA-modified nanochannels to CO_2 and N_2.

Notably, bubbling with CO_2 changes the pH of solution from 7.1 to 4.0, which may influence the conductivity of microfluidic[40] or nanofluidic channels. To exclude the mechanism of protonation, we changed the pH to 4.0 without the bubbling of CO_2. A rectification ratio of ~1.64, which is much lower than the former ratio 4.60 of the DEPBA-modified system, indicates that simply changing the pH to 4.0 does not lead to obvious current rectification. This finding confirms that the rectification is induced by the chemical reaction of amidine

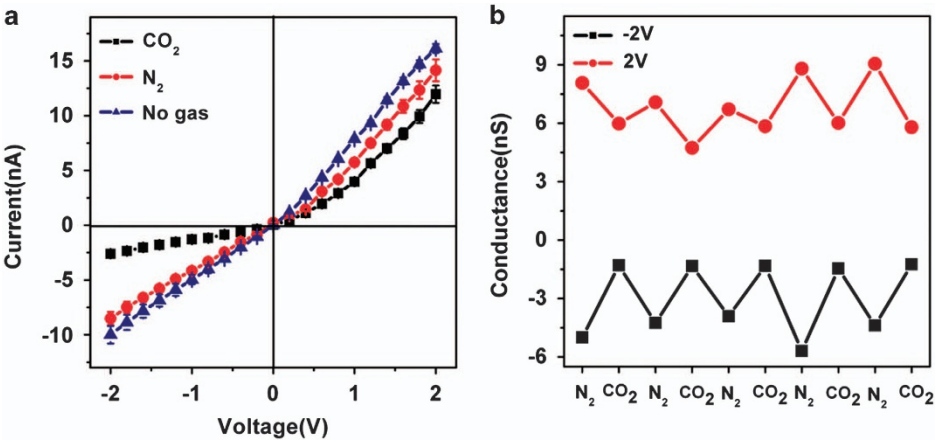

Figure 3 Reversible switchable multiple nanochannels. (**a**) *I–V* curves of CO_2 and N_2 bubbling in DEPBA-modified nanochannels. (**b**) Reversible functionalized nanochannels exhibit conductance with CO_2 bubbling and N_2 bubbling for the removal of CO_2 at 2 and − 2 V.

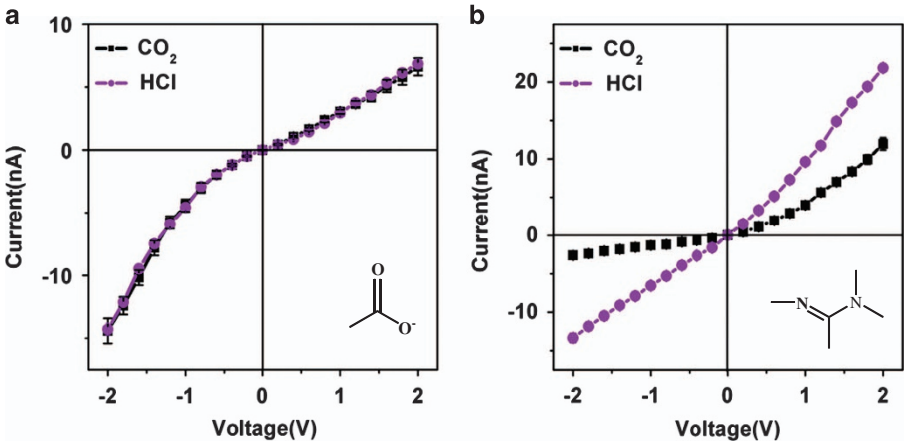

Figure 4 The current–voltage *(I–V)* curves of the nanochannel with different chemical components when bubbling with CO_2 and pH to 4.0 solutions. (**a**) The carboxyl groups are on the surface. (**b**) The amidine groups are on the surface. We observe different current rectification properties by bubbling with CO_2 and adjusting the solution to the same pH 4.0 when the surface is covered by amidine groups. When the surface is covered by carboxyl groups, the effects from CO_2 and pH are the same.

groups with CO_2. The pH difference will certainly change the conductive property of the nanochannels, but it is not the major factor to induce the current rectification. In addition, the CO_2-specific rectification is further confirmed by our controlled experiments of the nanochannels with different chemical components. First, when the surface of the nanochannels is covered by carboxyl groups, bubbling with CO_2 and adjusting the pH to 4.0 have the same effect on the conductance state (Figure 4a). Second, when the surface of the nanochannels is covered by amine groups, bubbling with CO_2 leads to the reversion of the current rectification direction, which is the same effect as adjusting the pH to 4.0 (Supplementary Figure S8). Third, only when the surface is modified with amidine groups, the effects caused by bubbling with CO_2 and by adjusting solution to the same pH 4.0 are apparently different (Figure 4b). The above results successfully demonstrate that CO_2 essentially induces ion current rectification by direct chemical reaction rather than pH change.

The ion rectification of DEPBA-modified nanochannels, which can capture CO_2 by amidine groups on the channel surface, sees a significant increase from 1.61 to 4.60 (increasing by 185%) when bubbling CO_2 to nanochannels, whereas the rectification of nanochannels covered with amino groups only shows a change from 1.53 to 2.59 (increasing by 69%). Supplementary Figure S9 shows that nanochannels covered with amidine groups exhibit a better improvement in the ion rectification than that of nanochannels with amino groups.

HCO_3^- is a byproduct of the CO_2 reaction. Here we introduce HCO_3^- in solution without CO_2 bubbling to verify the effect of HCO_3^- to rectification. The *I–V* curves in Supplementary Figure S10 indicate that the HCO_3^- solution does not induce ion current rectification and that the artificial smart system is selective to anions after direct reactions with CO_2 rather than HCO_3^-. Hence, the effect of HCO_3^- can be excluded.

The dependency of ion current properties on the duration of bubbling CO_2 to nanochannels was explored to further understand the effect of CO_2 volume to nanochannels. Figure 5a shows the ion current evolution with the binding of CO_2 to nanochannels before modification. Before bubbling CO_2, the ion current reaches ~ 9.56 nA at 2 V and ~ − 30.52 nA at − 2 V, and the corresponding current rectification ratio is ~ 0.31. With continuous bubbling CO_2 for 5 min, the ion current reaches ~ 8.24 nA at 2 V and ~ − 23.42 nA at − 2 V; the gating ratio is ~ 0.97, and the current rectification ratio is ~ 0.36. The ion gating ratio is defined as the ratio between the ion current

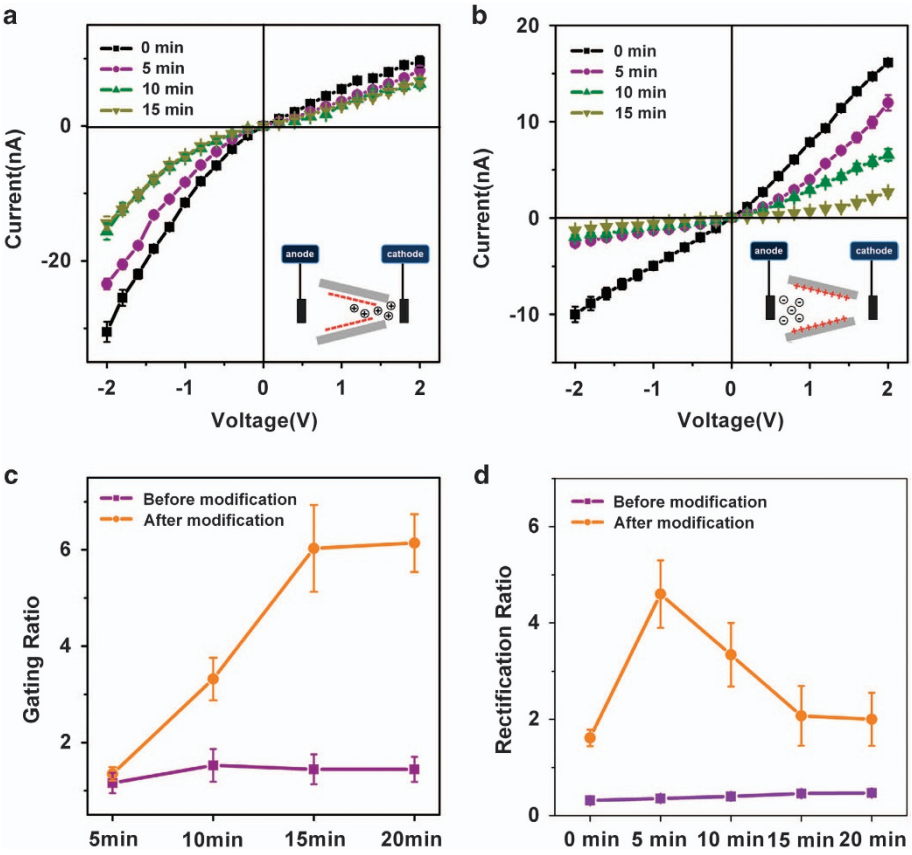

Figure 5 The current–voltage *(I–V)* curves of gas-responsive functionalized DEPBA-modified nanochannels (**a**) before and (**b**) after modification when bubbling CO_2 for different times. (**c**) The CO_2-activated gating ratio of nanochannels at −2 V voltage before and after modification. (**d**) Ion rectification ratio of gas-responsive nanochannels before and after modification. DEPBA, 4-[4-(1-dimethylamino-ethylideneamino)-phenyl-butyric acid.

values at +2 V before (I_1) and after (I_2) bubbling with CO_2 (that is, gating ratio $=I_1/I_2$).[41] After 10 min, the ion current remains ~6.26 nA at 2 V and ~−15.64 nA at −2 V; the gating ratio is ~1.52, and the current rectification ratio remains ~0.40. We found that the pristine negatively charged carboxyl groups attract cations, resulting in current rectification. With continuous CO_2 treatment, the ion currents decreased at both negative and positive voltages. Figure 5b shows the corresponding *I–V* curves of nanochannels after modification with amidine groups and the bubbling time of CO_2 varying from 0 to 15 min. Before bubbling CO_2, the rectification behavior of nanochannels vanishes because the immobilized DEPBA molecule is neutral. Bubbling CO_2 for 5 min causes ion current rectification as a result of the surface charge from neutral to positive. The ion current reaches ~11.96 nA at 2 V and ~−2.60 nA at −2 V; the current rectification ratio reaches a maximum of ~4.60, implying that a number of chemical-driven protonated species form in the nanochannels, and the gating ratio reaches ~1.45. When bubbling CO_2 for 10 min, ion current reaches ~6.56 nA at 2 V and ~−1.96 nA at −2 V; the current-rectification ratio reduces to ~3.34, and the gating ratio increases to ~3.39. With the continuous 15 min of bubbling CO_2, the ion current reaches ~2.67 nA at 2 V and ~−1.69 nA at −2 V. The current rectification ratio declines and finally reaches a stable value of ~2.07, and the gating ratio increases to ~6.01. At first, the current rectification ratio increases because the surface charge is strengthened in the appropriate concentration of CO_2. Then, the current rectification ratio decreases, indicating that the influence brought by forming bicarbonate in solution in the excess concentration of CO_2 partially neutralizes the amidine cation.

Using the same methods as for DEPBA-modified nanochannels, the ion transport properties of the DEDA-modified nanochannels were also investigated. Supplementary Figure S11 shows the *I–V* properties of the nanochannels before and after CO_2 treatment. The linear *I–V* curves of the nanochannels exhibit a tendency consistent with those of DEPBA-modified nanochannels. As shown in Supplementary Figures S11c and S11d, the maximum current rectification ratio of DEDA-modified nanochannels is ~2.21, and the gating ratio is ~1.32. These phenomena demonstrate that the ion current rectification property and the current change amplification of DEPBA-modified nanochannels are better than those of DEDA-modified nanochannels due to the less exposed surface charges in DEDA-modified nanochannels after being bubbled with CO_2.[42–44] A possible mechanism is shown in Figure 6.

In a CO_2 atmosphere, an important charge-switching process, from the neutral to the positive form of amidine groups in nanochannels, induces the intertangling of the long and flexible alkyl chains of DEDA, leading to the partial embedding of charges and the lower density of surface charges in the nanochannels (Figure 6a). By contrast, benefitting from its own relatively rigid aromatic structure, DEPBA retains its molecular conformation on the interior surface of nanochannels, offering more positive charges.[45] (Figure 6b).

The factor of gas pressure, which results from the nanopore radii, is also considered. It has been reported that nanopores with radii of ~200 nm rectified the current based on the gas pressure,[24,46]

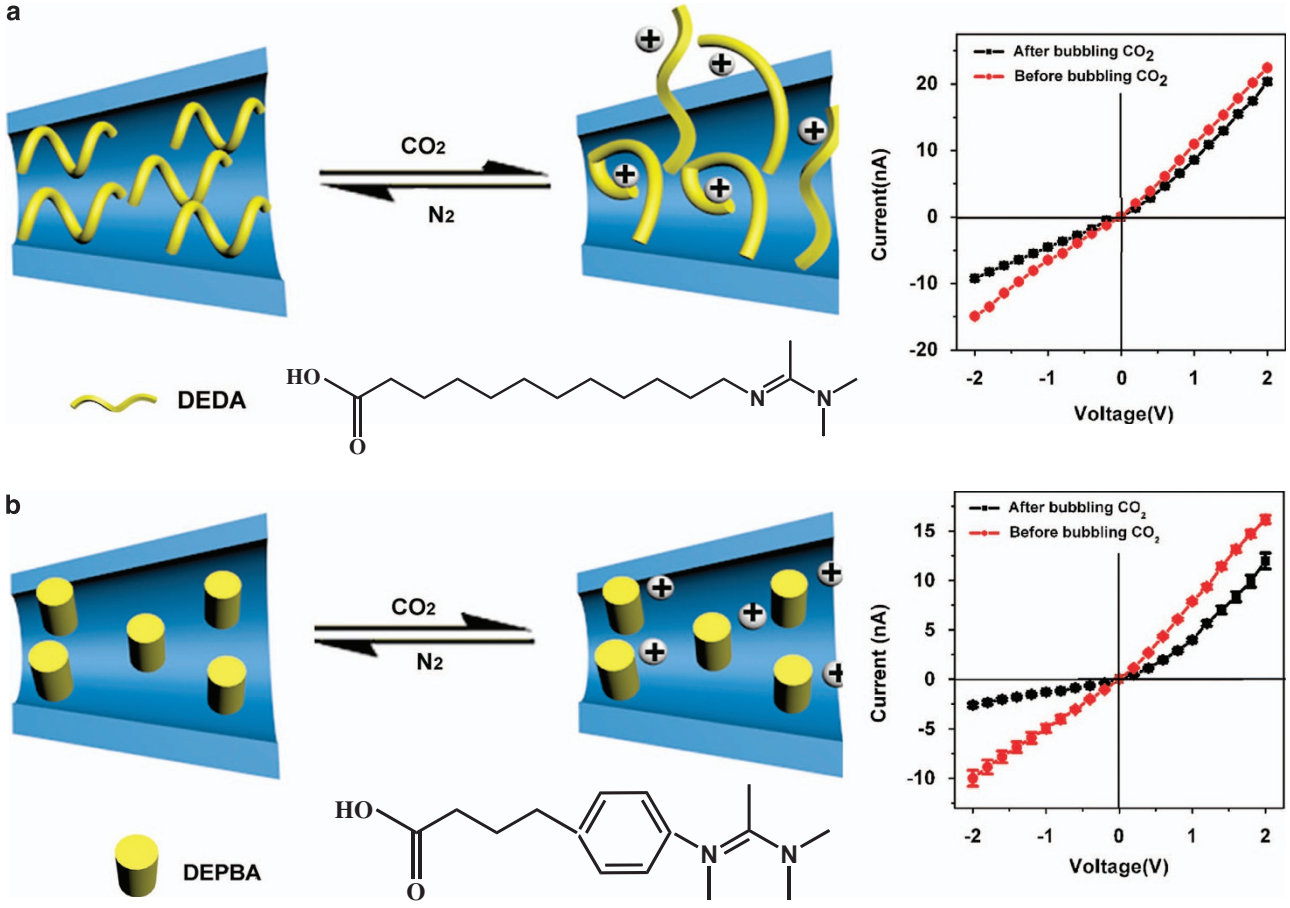

Figure 6 The molecular conformation change and current–voltage *(I–V)* curves before and after bubbling CO_2 to (**a**) DEDA-modified nanochannels and (**b**) DEPBA-modified nanochannels. DEDA, 12-(1-Dimethylamino-ethylideneamino)-dodecanoic acid; DEPBA, 4-[4-(1-dimethylamino-ethylideneamino)-phenyl-butyric acid.

whereas the geometrical structure of the nanopores with radii less than ~30 nm will have a negligible effect on the current. Thus, the possible mechanism of the physical gas pressures induced by CO_2 can be excluded for our smart chemical-driven nanopores because the radii of the nanopores in our system are <30 nm (Supplementary Figure S12).

DISCUSSION

To further investigate the reaction mechanism and simulate the non-linear ion current rectification behavior, four groups of mathematics model based on the PNP[47] equations were developed. Three groups of mathematic models correspond to the different times of bubbling CO_2 to nanochannels. Different surface charge densities of the nanopores are chosen: $6\times10^{-6}\,\mathrm{C\,m^{-2}}$, $4\times10^{-6}\,\mathrm{C\,m^{-2}}$, $2\times10^{-6}\,\mathrm{C\,m^{-2}}$.

The equations of Nernst–Plank are

$$J_i = -D_i(\nabla c_i + z_i\, c_i\, \nabla\varphi) + c_i v_{\mathrm{eof}},\ i = +,-$$

($i=+$ stands for cations, and $I=-$ stands for anions) together with the steady-state continuity equation and the Poisson equation, $\nabla J_i = 0$, $i=+,-$

$$\nabla^2\varphi = \frac{F^2}{\varepsilon RT}(C_- - C_+)$$

where J_i is the flux of ions, D_i is the diffusion coefficient, z_i is the charge number of ionic species i, φ denotes the local dimensionless electric potential, and c_i refers to the concentration of species i. v_{eof} is electroosmotic velocity. Using the software COMSOL Multiphysics, we combine the models of electrostatics (refer to the Poisson equations and surface charge density) and the transport of diluted species (refer to the Nernst–Planck equations) to simulate the ion current rectification process of this conical nanochannel.[39] Supplementary Figure S13 shows boundary conditions: The potential is applied to Side 1, changing from −2 to 2 V, $\nu = 1\,\mathrm{V\,s^{-1}}$, and Side 7 is grounded. The volume of the two cells is larger than that of nanochannels, so we assume that the surface of cells has no influence on ion transport. Sides 2, 3, 5 and 6 are set to a neutral surface; the surface charge densities of Sides 4 and 10 are $6\times10^{-6}\,\mathrm{C\,m^{-2}}$, $4\times10^{-6}\,\mathrm{C\,m^{-2}}$ and $2\times10^{-6}\,\mathrm{C\,m^{-2}}$, according to the external environment. The conical shape of the channel contributes to the asymmetric distribution of ions near the surface. The thickness (T) of the membrane is 2.3 μm. We assume that concentrations of ion in the same axial position are also the same for simplification, and we study only the ion concentration in the middle of the channel, along with the axial.

For the parameters, we set the boundary conditions of concentration to $c_L = c_R = 0.1$ M, which is the electrolyte solution concentration in our experiment. The diffusion coefficient is $D_+ = -1.95\times10^{-5}\,\mathrm{cm^2\,s^{-1}}$, which corresponds to the diffusion coefficient of $D_+ = 1.95\times10^{-5}\,\mathrm{cm^2\,s^{-1}}$ and $D_+ = 2.03\times10^{-5}\,\mathrm{cm^{-2}\,s^{-1}}$. The net surface charge of the nanochannel along the pore axis can range from $6\times10^{-6}\,\mathrm{C\,m^{-2}}$, $4\times10^{-6}\,\mathrm{C\,m^{-2}}$ to $2\times10^{-6}\,\mathrm{C\,m^{-2}}$,

according to the external environment.[48] In this case, the surface charge is due to the incomplete chemical reaction of amidine groups.[26]

Figure 7a shows the simulated *I–V* curves; obviously, the ion rectification is obtained when the CO_2 is applied. The rectification ratio reaches 2.39, which is comparable to 4.60, 2.88 and 2.07 obtained in the experiment. When increasing the ventilation of excess CO_2, there is a reaction of bicarbonate that partially neutralizes the amidine cation, resulting in a decreasing surface charge on the pore wall, and the current decreases in the *I–V* curve.

Figure 7b illustrates the electric potential distribution in the nanochannel at −2 and 2 V after bubbling with CO_2 at the net surface charge density of 6×10^{-6} C m^{-2}. It can be noted that the positive surface charge plays a key role in the electric potential distribution. At 2 V (the anode faces the tip of the nanochannel, and the cathode faces the base region), cations will be driven to the base region (cathode), and anions will be driven to the tip region (anode). With the positive surface charge, at the tip region, cations are repelled (facile to go to the base region), and anions are attracted (facile to go to the tip region) due to the electric static potential. This will increase the conductance and the ion current. At −2 V (the cathode faces the tip of the nanochannel), the situation is reversed. Cations will be driven to the left tip region, which will decrease the conductance and the ion current. Therefore, the rectification ratio exceeds 1.0 for this nanochannel, which is in good accordance with our experimental results.

Figures 7c and d show the anion concentration distribution along the central axis of the nanochannel after bubbling with CO_2 at the net surface charge density of 6×10^{-6} C m^{-2}. The zone near the tip has a radius in the scale of the electric double layer, resulting in higher conductance near the tip. Due to the positive surface charge, the accumulation of anions near the tip is achieved. The region where the anion concentration greatly varies is magnified (Figures 7a and b). The net surface charge is positive, and anions are the majority carriers. With an externally applied voltage, the electric field direction controls the ions, which will also contribute to the accumulation of anions. Apparently, the anions accumulate to a higher degree when a positive voltage is applied than when a negative voltage is applied. Therefore, the conical shape of the nanochannel contributes to the asymmetric distribution of ions near the surface,[39] which is the quantitative explanation for the ultimate current rectification property.

In summary, we report CO_2-induced ionic current rectification in the gas–liquid–solid three-phase interactions. The current rectification is induced directly by the chemical reaction of the functional molecule modified on the interior of the nanochannels with CO_2, rather than

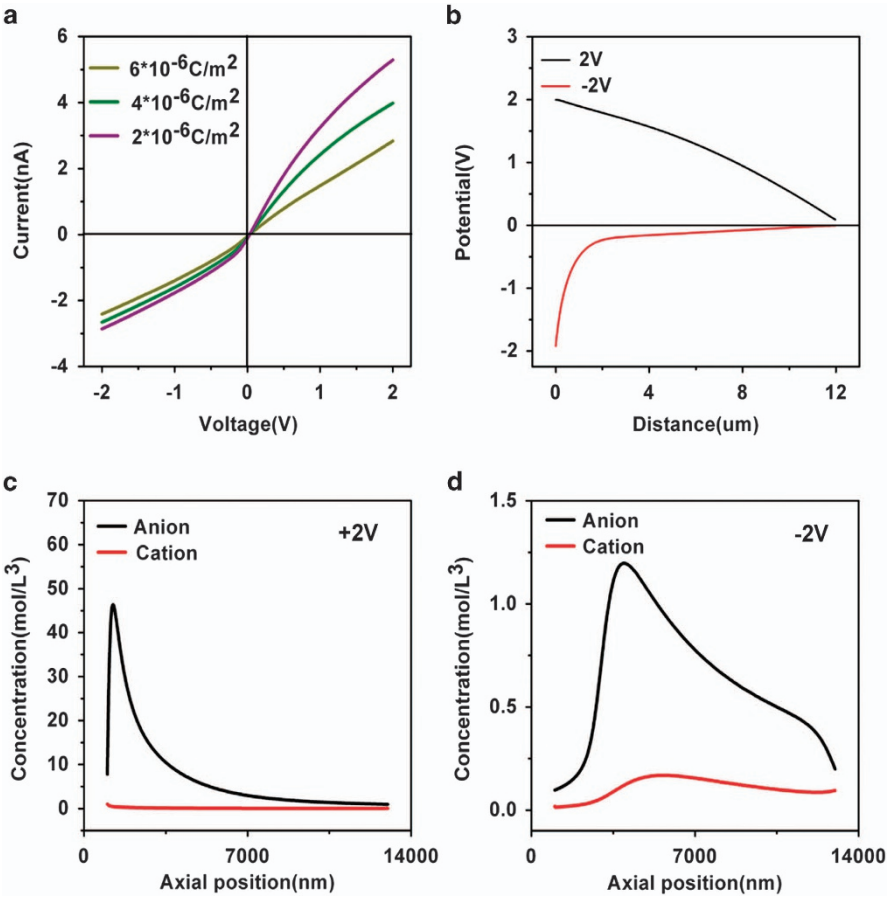

Figure 7 (**a**) Simulated current–voltage *(I–V)* curve of the nanochannel with increasing bubbling with CO_2. The simulated results accord with the experimental results based on the Poisson and Nernst–Planck equations. (**b**) Potential distribution in the nanochannel when the external applied voltage is −2 and 2 V after bubbling with CO_2. The positive surface charge plays a key role in the electric potential distribution, which leads to the nonuniformity of anion concentration distribution. (**c**) Anion concentration distribution along the nanochannel at −2 V after bubbling with CO_2. (**d**) Anion concentration distribution along the nanochannel at 2 V after bubbling with CO_2. Anion concentration accumulates to a higher degree at 2 V (46 M) than at −2 V (1.2 M) near the tip of the nanochannel. Therefore, the conductance is higher when the positive voltage is applied, which is the quantitative explanation of the current rectification property of this artificial CO_2-induced and chemical-driven smart nanochannel.

on the pH change. The effect of the different molecular conformation of the amidine-containing molecules on the current was investigated. Furthermore, the conclusive simulation results, which employ the PNP model, are highly similar to the experimental results. The recognition of CO_2 gas has become one of the most urgent research topics in fields related to energy and the environment. Therefore, we believe that these results not only demonstrate a preliminary step to mimic the complex gas–ion interaction during the photosynthesis process but also can help facilitate an understanding of the mechanism of the CO_2 activation process in biology.

CONFLICT OF INTEREST

The authors declare no conflict of interest.

ACKNOWLEDGEMENTS

We thank Kefeng Wang (BUAA) for beneficial discussions. We thank Tandre Oye (UCLA) for modifying the language in detail. This work was supported by the National Research Fund for Fundamental Key Projects (2011CB935704, 2014CB931800), the National Natural Science Foundation of China (21271016, 51373005), Program for New Century Excellent Talents in University (NCET-10-0035), the Scientific Research Foundation for the Returned Overseas Chinese Scholars of Ministry of Education of China (2011127004) and the Fundamental Research Funds for the Central Universities.

1 Engineer, C. B., Ghassemian, M., Anderson, J. C., Peck, S. C., Hu, H. H. & Schroeder, J. I. Carbonic anhydrases, EPF2 and a novel protease mediate CO_2 control of stomatal development. *Nature* **513**, 246–250 (2014).
2 Guo, Z. N., Song, R., Moon, J. H., Kim, M., Jun, E. J., Choi, J., Lee, J. Y., Bielawski, C. W., Sessler, J. L. & Yoon, J. A benzobisimidazolium-based fluorescent and colorimetric chemosensor for CO_2. *J. Am. Chem. Soc.* **134**, 17846–17849 (2012).
3 Tumarkin, E., Nie, Z. H., Park, J. I., Abo Ihasani, M., Greener, J., Sherwood-Lollar, B., Günthere, A. & Kumacheva, E. Temperature-controlled 'breathing' of carbon dioxide bubbles. *Lab. Chip.* **11**, 3545–3550 (2011).
4 Negi, J., Matsuda, O., Nagasawa, T., Oba, Y., Takahashi, H., Kawai-Yamada, M., Uchimiya, H., Hashimoto1, M. & Iba, K. CO_2 regulator slac1 and its homologues are essential for anion homeostasis in plant cells. *Nature* **452**, 483–488 (2008).
5 Bertil, H. *Ionic Channels of Excitable Membranes*, (Sunderland: UK, 1984).
6 Vahisalu, T., Kollist, H., Wang, Y., Nishimura, N., Chan, W., Valerio, G., Lamminmäki, A., Brosché, M., Moldau, H., Desikan, R., Schroeder, J. & Kangasjärvi, J. slac1 is required for plant guard cell S-type anion channel function in stomatal signalling. *Nature* **452**, 487–493 (2008).
7 Hu, H. H., Boisson-Dernier, A., Israelsson-Nordström, M., Böhmer, M., Xue, S. W., Ries, A., Godoski, J., Kuhn, J. M. & Schroeder, J. I. Carbonic anhydrases are upstream regulators of CO_2-controlled stomatal movements in guard cells. *Nat. Cell Biol.* **12**, 87–95 (2010).
8 Chen, Y., Hu, H. L., Punta, M., Bruni, R., Hillerich, B., Kloss, B., Rost, B., Love, J., Siegelbaum, S. A. & Hendrickson, W. A. Homologue structure of the slac1 anion channel for closing stomata in leaves. *Nature* **467**, 1074–1082 (2010).
9 Ookata, K., Tojo, A., Suzuki, Y., Nakamura, N., Kimura, K., Wilcox, C. S. & Hirose, S. Localization of inward rectifier potassium channel Kir7.1 in the basolateral membrane of distal nephron and collecting duct. *J. Am. Soc. Nephrol.* **11**, 1987–1994 (2000).
10 Macrae, M. X., Blake, S., Mayer, M. & Yang, J. Nanoscale ionic diodes with tunable and switchable rectifying behavior. *J. Am. Chem. Soc.* **132**, 1766–1767 (2010).
11 Vlassiouk, I. & Siwy, Z. S. Nanofluidic diode. *Nano Lett.* **7**, 552–556 (2007).
12 Ali, M., Tahir, M. N., Siwy, Z., Neumann, R., Tremel, W. & Ensinge, W. Hydrogen peroxide sensing with horseradish peroxidase-modified polymer single conical nanochannels. *Anal. Chem.* **83**, 1673–1680 (2011).
13 Horrocks, B. R., Schmidtke, D., Heller, A. & Bard, A. Scanning electrochemical microscopy. 24. enzyme ultramicroelectrodes for the measurement of hydrogen peroxide at surfaces. *Anal. Chem.* **65**, 3605–3614 (1993).
14 Gouaux, E. & MacKinnon, R. Principles of selective ion transport in channels and pumps. *Science* **310**, 1461–1465 (2005).
15 Vlassiouk, I., Kozel, T. R. & Siwy, Z, S. Biosensing with nanofluidic diodes. *J. Am. Chem. Soc.* **131**, 8211–8220 (2009).
16 Meng, Z. Y., Bao, H., Wang, J. T., Jiang, C. D., Zhang, M. H., Zhai, J. & Jiang, L. Artificial ion channels regulating light-induced ionic currents in photoelectrical conversion systems. *Adv. Mater.* **26**, 2329–2334 (2014).
17 Jiang, Y. N., Liu, N. N., Guo, W., Xia, F. & Jiang, L. Highly-efficient gating of solid-state nanochannels by DNA supersandwich structure containing ATP aptamers: a nanofluidic IMPLICATION logic device. *J. Am. Chem. Soc.* **134**, 15395–15401 (2012).
18 Guan, W. H., Fan, R. & Reed, M. A. Field-effect reconfigurable nanofluidic ionic diodes. *Nat. Commun.* **2**, 506 (2011).
19 Hou, X., Guo, W. & Jiang, L. Biomimetic smart nanopores and nanochannels. *Chem. Soc. Rev.* **40**, 2385–2401 (2011).
20 Powell, M. R., Cleary, L., Davenport, M., Shea, K. J. & Siwy, Z. S. Electric-field-induced wetting and dewetting in single hydrophobic nanopores. *Nat. Nanotechnol.* **6**, 798–802 (2011).
21 Wu, J., Gerstandt, K., Zhang, H. B., Liu, J. & Hinds, B. J. Electrophoretically induced aqueous flow through single-walled carbon nanotube membranes. *Nat. Nanotechnol.* **7**, 133–139 (2012).
22 Powell, M. R., Sullivan, M., Vlassiouk, I., Constantin, D., Sudre, O., Martens, C. C., Eisenberg, R. S. & Siwy, Z. S. Nanoprecipitation-assisted ion current oscillations. *Nat. Nanotechnol.* **3**, 51–57 (2008).
23 Vlassiouk, I., Kozel, T. R. & Siwy, Z. S. Biosensing with nanofluidic diodes. *J. Am. Chem. Soc.* **131**, 8211–8220 (2009).
24 Lan, W. J., Holden, D. A. & White, H. S. Pressure-dependent ion current rectification in conical-shaped glass nanopores. *J. Am. Chem. Soc.* **133**, 13300–13303 (2011).
25 Boer, H. J. D., Eppinga, M. B., Wassen, M. J. & Dekker, S. C. A critical transition in leaf evolution facilitated the cretaceous angiosperm revolution. *Nat. Commun.* **3**, 1221 (2012).
26 Du, Q. S., Fan, X. W., Wang, C. H. & Huang, R. B. A possible CO_2 conducting and concentrating mechanism in plant stomata SLAC1 channel. *PLos ONE* **6** (2011).
27 Jessop, P. G., Heldebrant, D. J., Li, X. W., Eckert, C. A. & Liotta, C. L. Reversible nonpolar-to-polar solvent. *Nature* **436**, 1102–1102 (2005).
28 Liu, Y. X., Jessop, P. G., Cunningham, M., Eckert, C. A. & Liotta, C. L. Switchable surfactants. *Science* **313**, 958–960 (2006).
29 Yan, Q., Zhou, R., Fu, C. K., Zhang, H. J., Yin, Y. W. & Yuan, J. Y. CO_2-responsive polymeric vesicles that breathe. *Angew. Chem. Int. Ed.* **50**, 4923–4927 (2011).
30 Tian, T., Chen, X., Li, H., Wang, Y., Gao, L. & Jiang, L. Amidine-based fluorescent chemosensor with high applicability for detection of CO_2: A facile way to "see" CO_2. *Analyst* **138**, 991–994 (2013).
31 Wang, Y., Xu, H. & Zhang, X. Tuning the amphiphilicity of building blocks: controlled self-assembly and disassembly for functional supramolecular materials. *Adv. Mater.* **21**, 2849–2864 (2009).
32 Guo, Z. R., Feng, Y. J., He, S., Qu, M. Z., Chen, H. L., Liu, H. B., Wu, Y. F. & Wang, Y. CO_2-responsive "smart" single-walled carbon nanotubes. *Adv. Mater.* **25**, 584–590 (2013).
33 Li, N., Thia, L. & Wang, X. A CO_2-responsive surface with an amidine-terminated self-assembled monolayer for stimuli-induced selective adsorption. *Chem. Commun.* **50**, 4003–4006 (2014).
34 Apel, P. Y., Korchev, Y. E., Siwy, Z., Spohr, R. & Yoshida, M. Diode-like single-ion track membrane prepared by electro-stopping. *Nucl. Instrum. Meth. B* **184**, 337–346 (2001).
35 Scoggins, M. A rapid gas chromatographic analysis of diastereomeric diamines. *J. Chromatograph. Sci.* **13**, 146–148 (1975).
36 Li, X., Wang, Y. & Jiang, L. A supramolecular approach to probing the influence of micro-phase structure on gas permeability of block copolymer membranes. *Sci. Adv. Mater.* **5**, 719–726 (2013).
37 Ali, M., Nasir, S., Ramirez, P., Ahmed, I., Nguyen, Q. H., Fruk, L., Mafe, S. & Ensinger, W. Optical gating of photosensitive synthetic ion channels. *Adv. Funct. Mater.* **22**, 390–396 (2012).
38 Ali, M., Yameen, B., Cervera, J., Ramírez, P., Neumann, R., Ensinger, W., Knoll, W. & Azzaroni, O. Layer-by-layer assembly of polyelectrolytes into ionic current rectifying solid-state nanopores: insights from theory and experiment. *J. Am. Chem. Soc.* **132**, 8338–8348 (2010).
39 Ali, M., Ramirez, P., Mafe, S., Neumann, R. & Ensinger, W. A pH-tunable nanofluidic diode with a broad range of rectifying properties. *ACS Nano* **3**, 603–608 (2009).
40 Park, J. I., Nie, Z. H., Kumachev, A., Abdelrahman, A. I., Binks, B. P., Stone, H. A. & Kumacheva, E. A microfluidic approach to chemically driven assembly of colloidal particles at gas-liquid interfaces. *Angew. Chem. Int. Ed.* **48**, 5300–5304 (2009).
41 Bormann, J., Hamill, O. P. & Sakmann, B. Mechanism of anion permeation through channels gated by glycine and gamma-aminobutyric acid in mouse cultured spinal neurones. *J. Physiol.* **385**, 243–286 (1987).
42 Li, C. Y., Ma, F. X., Wu, Z. Q., Gao, H. L., Shao, W. T., Wang, K. & Xia, X. H. Solution-pH-modulated rectification of ionic current in highly ordered nanochannel arrays patterned with chemical functional groups at designed positions. *Adv. Funct. Mater.* **23**, 3836–3844 (2013).
43 Chen, W., Wu, Z. Q., Xia, X. H., Xu, J. J. & Chen, H. Y. Anomalous diffusion of electrically neutral molecules in charged nanochannels. *Angew. Chem. Int. Ed.* **49**, 7943–7947 (2010).
44 Li, S. J., Li, J., Wang, K., Wang, C., Xu, J. J., Chen, H. Y., Xia, X. H. & Huo, Q. A nanochannel array-based electrochemical device for quantitative label-free DNA analysis. *ACS Nano* **4**, 6417–6424 (2010).

45 Lahann, J., Mitragotri, S., Tran, T. N., Kaido, H., Sundaram, J., Choi, I. S., Hoffer, S., Somorjai, G. A. & Langer, R. A reversibly switching surface. *Science* **299**, 371–374 (2003).
46 Martinac, B., Buechner, M., Delcour, A. H., Adler, J. & Kung, C. Pressure-sensitive ion channel in *Escherichia coli*. *Proc. Natl Acad. Sci. USA* **84**, 2297–2301 (1987).
47 Constantin, D. & Siwy, Z. S. Poisson-Nernst–Planck model of ion current rectification through a nanofluidic diode. *Phys. Rev. E* **76**, 041202 (2007).
48 Siwy, Z. S. Ion-current rectification in nanopores and nanotubes with broken symmetry. *Adv. Funct. Mater.* **16**, 735–746 (2006).

Supplementary Information accompanies the paper on the NPG Asia Materials website (http://www.nature.com/am)